

Measurement of Arcminute Scale Cosmic Microwave Background Anisotropy with the BIMA Array

K.S. Dawson¹, W.L. Holzapfel¹, J.E. Carlstrom^{2,3},
 M. Joy⁴, S.J. LaRoque², A. Miller² and D. Nagai²

ABSTRACT

We report the results of our continued study of arcminute scale anisotropy in the Cosmic Microwave Background (CMB) with the Berkeley-Illinois-Maryland Association (BIMA) array. The survey consists of ten independent fields selected for low infrared dust emission and lack of bright radio point sources. With observations from the VLA at 4.8 GHz, we have identified point sources which could act as contaminants in estimates of the CMB power spectrum and removed them in the analysis. Modeling the observed power spectrum with a single flat band power with average multipole of $\ell_{eff} = 6864$, we find $\Delta T = 14.2^{+4.8}_{-6.0} \mu\text{K}$ at 68% confidence. The signal in the visibility data exceeds the expected contribution from instrumental noise with 96.5% confidence. We have also divided the data into two bins corresponding to different spatial resolutions in the power spectrum. We find $\Delta T_1 = 16.6^{+5.3}_{-5.9} \mu\text{K}$ at 68% confidence for CMB flat band power described by an average multipole of $\ell_{eff} = 5237$ and $\Delta T_2 < 26.5 \mu\text{K}$ at 95% confidence for $\ell_{eff} = 8748$.

Subject headings: cosmology: observation – cosmic microwave background

¹Department of Physics, University of California, Berkeley CA 94720

²Department of Astronomy and Astrophysics, University of Chicago, Chicago IL 60637

³Center for Cosmological Physics, Dept. of Physics, Enrico Fermi Institute, University of Chicago, Chicago, IL 60637

⁴Space Science Laboratory, SD50, NASA Marshall Space Flight Center, Huntsville AL 35812

1. Introduction

Fluctuations in the distribution of matter at the epoch of recombination create large angular scale anisotropy in the Cosmic Microwave Background (CMB). This primordial anisotropy has been studied extensively at degree and sub-degree angular scales in order to place constraints on the parameters of cosmological models (Halverson et al. 2002, de Bernardis et al. 2002, Lee et al. 2001, Miller et al. 2001, Padin et al. 2001). At arcminute scales, the primordial anisotropy is damped to negligible amplitude due to photon diffusion and the finite thickness of the last scattering surface (Hu & White 1997). On these smaller scales, secondary anisotropies such as the Sunyaev-Zeldovich (SZ) effect are expected to dominate the signal of the CMB power spectrum (Haiman & Knox 1999). Studies of secondary anisotropy in the CMB have the potential to be a powerful probe of the growth of structure in the Universe.

In this paper, we report results from an ongoing program using the Berkeley-Illinois-Maryland Association (BIMA) interferometer to search for arcminute-scale CMB anisotropy. Discussion of the instrument, data reduction, expected signals (from both primary and secondary anisotropies) and previous measurements is included in earlier publications (Holzapfel et al. 2000 and Dawson et al. 2001, hereafter H2000 and D2001 respectively). We describe observations and criteria for field selection in §2. The Bayesian likelihood analysis used to constrain the CMB anisotropy is described in §3. The results are presented in §4 including a discussion of tests for systematic errors in the analysis. Finally, in §5, we present the conclusion and prospects for future work.

2. Observations

Analysis of eleven fields observed with the BIMA array during the summers of 1997, 1998, and 2000 revealed a significant detection of excess power (D2001). In an effort to achieve uniform sensitivity and selection criteria across our sample, we continued the project in the summer of 2001 with a subset of eight fields from the original survey. Two new fields were also added to the survey for a total of ten. Each field was observed with the BIMA array and the Very Large Array (VLA)⁵.

⁵The VLA is operated by the National Radio Astronomy Observatory, a facility of the National Science Foundation, operated

2.1. Field Selection

The two new fields added to the survey, BDF12 and BDF13, lie at Right Ascensions convenient for summer observations and outside of the galactic plane. This makes for a total of ten independent fields for the survey in 2001, covering approximately 0.1 square degrees. The fields were selected from the *IRAS* 100 μ m and VLA NVSS (Condon et al. 1998) radio surveys to lie in regions with low dust contrast and no bright radio sources. In addition, we used SkyView to access digitized sky survey and ROSAT images to check for bright optical or x-ray emission which could complicate follow-up observations. The pointing centers for each of the ten fields are given in Table 1.

Two of the fields used in the D2001 analysis, PC1643+46 and VLA1312+32, were originally selected to follow-up previously reported microwave decrements (Jones et al. 1997; Richards et al. 1997). A third field, in the direction of the high redshift quasar PSS0030+17, was originally selected as a distant cluster candidate. These three fields did not follow the same selection criteria as the rest of the fields and are not included in the present sample. Since observations of these fields are not as deep as those for the other blank fields, removing them from the survey does not have a significant effect on the results reported in this paper.

2.2. BIMA Observations

A priority for 2001 observations was to achieve uniform flux sensitivity across our sample of ten fields. We re-observed fields from the previous years and dedicated 55 hours to each of the new fields, aiming for a uniform noise level of $< 150 \mu\text{Jy}/\text{beam RMS}$ on short baselines ($u-v < 1.1 \text{k}\lambda$) for each field in the sample. This noise level corresponds to $\sim 15 \mu\text{K}$ RMS for a 2' synthesized beam.

All anisotropy observations were made using the BIMA array at Hat Creek. Nine 6.1 meter telescopes of the array were equipped for operation at 28.5 GHz, providing a 6.6' FWHM field of view. In order to track phase and gain fluctuations, all field observations were bracketed by observations of bright radio point sources (H2000). The fluxes of these calibration sources are all referenced to the flux of Mars which is uncertain by approximately 4% at 90% confidence (see discussion in Grego 2000). This uncertainty is

under cooperative agreement by Associated Universities, Inc.

small compared to the uncertainty in the anisotropy signals we report here and therefore makes a negligible contribution to the uncertainties in the reported results. The cumulative integration time for each of the ten fields observed in this survey is listed in Table 1. After calibration and data edits, a total of 607 hours of integration have been dedicated to this project.

2.3. VLA Observations and Point Source Results

Sources of foreground emission have the potential to contaminate estimates of the CMB power spectrum. Contaminants at 28.5 GHz arising from galactic sources such as dust, synchrotron, and free-free emission are expected to be below the μK level at arcminute angular scales in the regions of the sky selected for this survey. However, emission from radio point sources could contribute significantly to excess power in the observations described here (e.g. Tegmark et al. 2000).

The compact configuration used for the BIMA anisotropy observations was designed to produce high sensitivity to extended sources. However, this configuration has limited sensitivity on the long baselines which in principle could be used to locate and remove point sources. To help constrain the contribution from point sources to the anisotropy measurements, we used the VLA at a frequency of 4.8 GHz to observe each field in the survey. With 1.5 hours per field, these observations yielded an RMS flux of $\sim 25 \mu\text{Jy}/\text{beam}$ for a $9'$ FWHM region with the same pointing center as a BIMA field. The positions of all point sources with flux $> 6\sigma$ within $8'$ of the pointing center have been recorded. Measured point sources with fluxes corrected for attenuation from the primary beam at 4.8 GHz are listed in Table 2. If the spectra of the point sources are flat or falling, deep observations with the VLA will identify those that lie at or below the noise level in the 28.5 GHz maps.

3. Analysis

The analysis in this paper is similar to that used to produce the previous BIMA anisotropy results and is based on the formalism presented in White et al. (1999) for the determination of the CMB power spectrum from interferometer data. We bin the visibility data and calculate joint confidence intervals as described in H2000. The likelihood function to test a

theory for a set of bandpowers, $\{C_\ell$, with n measured visibilities is defined

$$\mathcal{L}(\{C_\ell\}) = \frac{1}{\pi^n \det C} \exp \left[-V^*(\mathbf{u}_i) C_{ij}^{-1} V(\mathbf{u}_j) \right] , \quad (1)$$

where C_{ij} is the correlation matrix of visibilities at \mathbf{u}_i and \mathbf{u}_j .

There are several changes from the analysis in H2000. We first perform the analysis on a single band-power with data spanning the u - v range $0.63 - 1.7 \text{ k}\lambda$. We then perform an analysis with data divided into two bins, $0.63 - 1.1 \text{ k}\lambda$ and $1.1 - 1.7 \text{ k}\lambda$, corresponding to different spatial resolution. A constraint correlation matrix is introduced to account for the point sources identified with the VLA. In this new formalism, the correlation matrix can be represented as

$$C_{ij} = C_{ij}^V + C_{ij}^N + C_{ij}^C , \quad (2)$$

where C_{ij}^V represents the theory correlation matrix, C_{ij}^N represents the noise correlation matrix, and C_{ij}^C represents the constraint correlation matrix used to remove the effect of point sources from the determination of the CMB power spectrum.

3.1. Theory Correlation Matrix

The fundamental tool for analysis of Gaussian temperature fluctuations is the theory correlation matrix. The theory correlation matrix is calculated from the observed visibilities measured at a set of points \mathbf{u}_i . The measured flux densities are given by

$$V(\mathbf{u}) = \frac{\partial B_\nu}{\partial T} \int d\mathbf{x} \Delta T(\mathbf{x}) A(\mathbf{x}) e^{2\pi i \mathbf{u} \cdot \mathbf{x}} , \quad (3)$$

where $\Delta T(\mathbf{x})$ is the temperature distribution on the sky, $A(\mathbf{x})$ is the primary beam of the telescope,

$$\frac{\partial B_\nu}{\partial T} = 2k_B \left(\frac{k_B T}{hc} \right)^2 \frac{x^4 e^x}{(e^x - 1)^2} , \quad (4)$$

k_B is Boltzmann's constant, and $x \equiv h\nu/k_B T_{\text{cmb}}$. Following White et al. (1999), we define the visibility correlation matrix,

$$\begin{aligned} C_{ij}^V &\equiv \langle V^*(\mathbf{u}_i) V(\mathbf{u}_j) \rangle \\ &= \left(\frac{\partial B_\nu}{\partial T} \right)^2 \int_0^\infty w dw S(w) W_{ij}(w) , \end{aligned} \quad (5)$$

which is proportional to the product of the power spectrum, $S(w)$, and the visibility window function.

The window function is given by

$$W_{ij}(|\mathbf{w}|) \equiv \int_0^{2\pi} d\theta_w \tilde{A}^*(\mathbf{u}_i - \mathbf{w}) \tilde{A}(\mathbf{u}_j - \mathbf{w}) , \quad (6)$$

where $\tilde{A}(\mathbf{u})$ is the Fourier transform of the telescope primary beam. In the case of a single flat band power and $\ell > 60$, we can write

$$C_{ij}^V = \frac{1}{2\pi} \left(\frac{\partial B_\nu}{\partial T} \right)^2 \Delta T^2 \int_0^\infty \frac{dw}{w} W_{ij}(w) , \quad (7)$$

where

$$\Delta T^2 \equiv \frac{T_{CMB}^2}{2\pi} C_\ell \ell(\ell + 1) \quad (8)$$

is the RMS of the CMB anisotropy contributed by the power spectra C_ℓ . In general, the theory can be expressed as a function of bandpowers. The most likely values and confidence intervals are calculated for each band independently by integrating the likelihood function

$$\mathcal{L}(\{C_{\ell m}\}) = \sum_{C_{\ell 1}} \cdots \sum_{C_{\ell m-1}} \sum_{C_{\ell m+1}} \cdots \sum_{C_{\ell n}} \mathcal{L}(\{C_{\ell 1} \cdots C_{\ell n}\}) \quad (9)$$

For the analysis of a single bin of visibility data in the u - v range $0.63 - 1.7 \text{ k}\lambda$, the likelihood is only calculated over one variable, as in H2000 and D2001. For the analysis in this work, it is assumed that $\Delta T^2 \geq 0$ and for visibility data in the u - v range $1.7 - 3.0 \text{ k}\lambda$, $C_{ij}^V = 0$.

3.2. Noise Correlation Matrix

As with most interferometric observations, the system temperature of the receivers in the BIMA array is continuously monitored. Each visibility is assigned an estimated uncertainty

$$\sigma_{raw,i}^2 = \left(\frac{2k_B T_{sys,i}}{\eta A} \right)^2 \frac{1}{\Delta_\nu t} , \quad (10)$$

where $T_{sys,i}$ is the system temperature for the visibility $V(\mathbf{u}_i)$, η is the aperture efficiency, A is the area of the telescope, Δ_ν is the effective bandwidth, and t is the integration time. The values of $T_{sys,i}$, η , and Δ_ν are known within a few percent. The noise is rescaled independently for each baseline. The reduced χ^2 is calculated from each visibility, j , recorded from a given baseline

$$\chi^2 = \sum_j \frac{V^*(\mathbf{u}_j) V(\mathbf{u}_j)}{\sigma_{raw,j}^2} . \quad (11)$$

The noise for that baseline is then rescaled so that $\sigma_j^2 = \frac{\sigma_{raw,j}^2}{\chi^2}$. The noise correlation matrix is calculated from the rescaled noise for each baseline as in H2000, $C_{ii}^N = \frac{1}{\sigma_i^2}$. With approximately 3000 visibilities per baseline, the expected error in the rescaled noise due to sample variance is $\sim 1.8\%$ on a single baseline. In order to test what effect this uncertainty has on the analysis, we both increased and decreased each term in the noise correlation matrix by 2% and found no significant change in estimates of excess power.

3.3. Constraint Correlation Matrix

As discussed in D2001, the effectiveness of subtracting point sources directly from the visibility data is limited with the compact configuration of the BIMA array. Using the VLA at 4.8 GHz, we can identify the positions of point sources which might contaminate the visibility data. We introduce a constraint correlation matrix (Bond et al. 1998) to marginalize over point source fluxes as in Halverson et al. (2002). Using this formalism, it is necessary only to identify the position of a potential source and not its flux.

Each point source is represented with a template Λ_{ni} of unknown amplitude κ_n for each visibility $V(\mathbf{u}_i)$ where the subscript, n , corresponds to the n th point source. The template is derived from the response of the visibilities to a point source that is offset from the pointing center by ΔRA_n , ΔDEC_n for a baseline, $(\mathbf{u}_i, \mathbf{v}_i)$

$$\Lambda_{ni} = e^{2\pi i (u_i \Delta RA_n + v_i \Delta DEC_n)} . \quad (12)$$

The constraint correlation matrix can be expressed

$$C_{ij}^C = \sum_{n,n'} \Lambda_{ni} \kappa_n \Lambda_{n'j} \kappa_{n'} , \quad (13)$$

where n and n' are each summed over the number of point sources in the field. In the limit $\kappa_n \kappa_{n'} \rightarrow \infty$, this procedure effectively assigns zero weight to modes within the visibility data that correspond to point source positions identified with the VLA. To avoid singularities in the inverted correlation matrix, a finite, but large ($\kappa_n \kappa_{n'} \gg \langle C_{ii}^N \rangle$) value is assigned to the point source amplitude. A value of $\kappa_n \kappa_{n'} \sim 10^4 \langle C_{ii}^N \rangle$ has been assumed in the analysis; the results are insensitive to the exact value of $\kappa_n \kappa_{n'}$.

Although some fields were observed in 1998 with longer baselines, most fields in this survey were observed from the compact configuration. The compact

configuration of the BIMA array was contained within a u - v radius of $3.0 \text{ k}\lambda$. These baselines are included in order to achieve a reasonable level of discrimination between the signature of a point source and the CMB anisotropy described in §3.1. In this manner, we remove the contribution to the measured power from linear combinations of baselines that may be corrupted by point source emission. With each additional point source constraint, a degree of freedom is lost and the uncertainty in the measured power increases accordingly.

4. Results

We have produced and analyzed images for each of the observed fields. The statistics of the images are described in Table 3 ($0.63 - 1.7 \text{ k}\lambda$), 4 ($0.63 - 1.1 \text{ k}\lambda$), and 5 ($1.1 - 1.7 \text{ k}\lambda$). The reported RMS values are those expected from the noise properties of the visibilities. The RMS temperature measurement corresponds to the synthesized beamsize for the given uv coverage. The baselines used to produce the image statistics are the same as the baselines included in the two bins of visibility data for the CMB anisotropy analysis. The window function produced from the noise weighted sum of the window functions for the individual visibilities in the u - v range $0.63 - 1.1 \text{ k}\lambda$ has an average value of $\ell_{\text{eff}} = 5237$ with FWHM $\ell = 2870$. The window function for visibilities in the u - v range $1.1 - 1.7 \text{ k}\lambda$ has an average value $\ell_{\text{eff}} = 8748$ with FWHM $\ell = 4150$. For the analysis using a single bin of data in the u - v range $0.63 - 1.7 \text{ k}\lambda$, $\ell_{\text{eff}} = 6864$ with FWHM $\ell = 6800$. The window functions for all three bands are plotted as a function of multipole in Figure 1.

4.1. Measurement of Anisotropy

We present the results of the analysis of the BIMA data assuming a CMB power spectrum that is described by one or two flat band powers. In Tables 3, 4, and 5, we show the most likely ΔT with confidence intervals for each of the ten fields included in this survey. Results for the joint likelihood for all the data are also included. Figure 2 shows the relative likelihoods as a function of assumed ΔT for a combined likelihood analysis of the ten fields. The results are normalized to unity likelihood for the case of no anisotropy signal. The measured signal exceeds that expected from instrument noise with 97.8% confidence for data which falls in the u - v range $0.63 - 1.1 \text{ k}\lambda$ and with 96.5% con-

fidence for the single bin of visibility data that covers the u - v range $0.63 - 1.7 \text{ k}\lambda$.

We include a contour plot of the two dimensional likelihood function in Figure 3 in order to demonstrate the correlation between the two flat band power bins. Contours represent 68%, 95%, and 99% confidence intervals. We calculate the correlation matrix, F , between the two bandpower bins directly from the likelihood function,

$$\begin{pmatrix} \langle (\Delta T_1 - \overline{\Delta T}_1)^2 \rangle & \langle (\Delta T_1 - \overline{\Delta T}_1)(\Delta T_2 - \overline{\Delta T}_2) \rangle \\ \langle (\Delta T_2 - \overline{\Delta T}_2)(\Delta T_1 - \overline{\Delta T}_1) \rangle & \langle (\Delta T_2 - \overline{\Delta T}_2)^2 \rangle \end{pmatrix} \quad (14)$$

$$F = \begin{pmatrix} 3.738 \times 10^{-11} & 1.448 \times 10^{-11} \\ 1.448 \times 10^{-11} & 1.920 \times 10^{-10} \end{pmatrix} (\mu K)^2 \quad . \quad (15)$$

This matrix can be diagonalized with eigenvalues

$$F' = \begin{pmatrix} 3.604 \times 10^{-11} & 0 \\ 0 & 1.933 \times 10^{-10} \end{pmatrix} (\mu K)^2 \quad , \quad (16)$$

and corresponding eigenvectors, $\mathbf{X}'_1 = 0.996\mathbf{X}_1 + 0.0893\mathbf{X}_2$ and $\mathbf{X}'_2 = 0.0893\mathbf{X}_1 - 0.996\mathbf{X}_2$. There is less than 10% correlation between the two bins of visibility data.

4.2. Systematics Check

We performed tests for systematic errors in all fields with significant excess power as described in D2001. Due to finite computing resources, the analysis is limited to visibility data in u - v range $0.63 - 1.1 \text{ k}\lambda$ described by ΔT_1 . The power in the second bin is fixed at $\Delta T_2 = 0$ for all tests described in this section. We tested for sources of contamination that change with time. Assuming that a terrestrial source, the sun, or the moon varies in position by several degrees over the course of a few days, such a local effect should be discovered from analysis of subsets divided into hours of observation or days of observation described in D2001. There was no significant difference in the measured power in subsets divided by day of observation or in the subsets divided by hour of observation.

We also added three additional tests this year to search for systematic errors in BDF12 and BDF13. We performed a jack-knife systematic test by breaking the data into subsets of four and five telescopes looking for antenna based systematic errors. For a test of baseline based systematic errors, we created

an east-west baseline subset and a north-south baseline subset. There was approximately the same level of excess power in each subset, as well as all of the subsets described in D2001. The third test combined the raw visibilities from observations of several different fields taken in a single summer to look for correlations between observations of independent fields. As would be expected for uncorrelated data, the analysis of the combined data sets revealed no significant excess power. Overall, we find no evidence that our results are biased by systematic effects.

As discussed in §2.3, we have adopted a VLA flux density limit of 6σ for identifying point sources. We now consider how different point source flux density limits affect our estimates of CMB anisotropy. We test the effect of four different point source models on the determination of the most likely ΔT_1 and confidence intervals. The results are found in Table 6. There is no significant difference in the ΔT_1 determined from the range of models considered. As in D2001, the flat band power results are insensitive to the details of the point source analysis.

5. Conclusion

Over the course of three summers, we have used the BIMA array in a compact configuration at 28.5 GHz to search for CMB anisotropy in ten independent $6.6'$ FWHM fields. With these observations, we have detected arcminute scale anisotropy at better than 95% confidence. In the context of an assumed flat band power model for the CMB power spectrum, we find $\Delta T = 14.2_{-6.0}^{+4.8} \mu\text{K}$ at 68.3% confidence with sensitivity on scales that correspond to an average harmonic multipole $\ell_{\text{eff}} = 6864$. We also present results after dividing the visibility data into two bins of different spatial resolution. We find $\Delta T_1 = 16.6_{-5.9}^{+5.3} \mu\text{K}$ at 68.3% confidence on scales corresponding to an average harmonic multipole $\ell_{\text{eff}} = 5237$ and $\Delta T_2 < 26.5 \mu\text{K}$ at 95% confidence at $\ell_{\text{eff}} = 8748$.

Mason et al. (2002) have also reported a detection of excess power at somewhat larger angular scales. They find $\Delta T = 22.5_{-3.6}^{+2.5} \mu\text{K}$ for data in the range $2010 < \ell < 4000$. Although this measurement is at a lower ℓ than the BIMA results, it is significantly higher than the expected power due to primordial anisotropy.

A possible explanation for the excess power at arcminute scales reported here is secondary anisotropy such as the SZ effect. Analytic models and simu-

lations of cluster formation predict ΔT values that range from $4.3 \mu\text{K}$ to $15.0 \mu\text{K}$ on the angular scales at which the BIMA experiment is sensitive. Figure 4 compares the results of this paper to several recent hydrodynamic simulations and analytic models of structure formation.

The non-Gaussian characteristics of the CMB power spectrum caused by the thermal SZ effect may increase the uncertainty in measurements of the power spectrum due to sample variance. Current models suggest that these effects increase the uncertainty by a factor of 3 over what is expected for the sample variance of a Gaussian distributed signal at $\ell \sim 5000$ (White, Hernquist, & Springel 2002). Based on this argument, the effect of non-Gaussian sample variance contributes a standard deviation of $3 \times \sqrt{2/N} \Delta T = 6.0 \mu\text{K}$ to the anisotropy measurements, where $N \sim 100$ is the number of independent pixels in the $u-v$ range $0.63 - 1.1 \text{ k}\lambda$ and $\sqrt{2/N} \Delta T$ is the sample variance in a Gaussian distributed signal. The uncertainty due to sample variance is approximately equal to the statistical uncertainty reported in this paper, increasing the overall uncertainty by 40%, in agreement with the predictions of Zhang, Pen & Wang (2002). The predicted effect of sample variance on the measurements is represented by the extended error bars in Figure 4.

We thank the entire staff of the BIMA observatory for their many contributions to this project, in particular Rick Forster and Dick Plambeck for their assistance with both the instrumentation and observations. Nils Halverson and Martin White are thanked for stimulating discussions concerning data analysis. We are grateful for the scheduling of time at the VLA in support of this project that has proved essential to the point source treatment. This work is supported in part by NASA LTSA grant number NAG5-7986, NSF grant 0096913, and the David and Lucile Packard Foundation. The BIMA millimeter array is supported by NSF grant AST 96-13998.

REFERENCES

Bond, J. R., Jaffe, A. H., & Knox, L. 1998, Phys Rev D57, 2117-2137.

Condon, J. J., Cotton, W. D., Greisen, E. W., Yin, Q. F., Perley, R. A. Taylor, G. B., & Broderick, J. J. 1998, AJ, 115, 1693.

Cooray A., 2000, PRD, 62, 103506.

Dawson, K. S., Holzapfel, W. L., Carlstrom, J. E., Joy, M., LaRoque, S. J., & Reese, E. D. 2001, ApJ, 553, L1.

de Bernardis, P. et al. 2002, ApJ, 564, 559.

Grego, L., Carlstrom, J.E., Reese, E.D., Holder, G.P., Holzapfel, W.L., Joy, M., Mohr, J.J., & Patel, S. 2000, ApJ, 552, 2.

Haiman, Z., & Knox, L. 1999, astro-ph/9902311.

Halverson, N.W. et al. 2002, ApJ, 568, 38.

Holder G.P., Carlstrom J.E., 1999, in Microwave Foregrounds, ed. de Oliveira-Costa A. and Tegmark M., p.199, ASP Conference Series, San Francisco

Holzapfel, W. L., Carlstrom, J. E., Grego, L., Holder, G., Joy, M., & Reese, E. D. 2000, ApJ, 539, 57.

Hu, W., & White, M. 1997, ApJ, 479, 568.

Jones et al. 1997, ApJ, 479, L1.

Komatsu E., Kitayama T., 1999, ApJ, 526, L1

Lee, A.T. et al. 2001, ApJ, 561, L7.

Mason, B.S. et al. 2002, submitted to ApJ, astro-ph/0205384.

Miller, A. et al. 2001, astro-ph/0108030.

Molnar S.M., Birkinshaw M., 2000, ApJ, 537, 542

Padin, S. et al. 2001, ApJ, 549, L1-L5.

Refregier A., Komatsu E., Spergel D.N., Pen U.-L., 2000, Phys. Rev. D, 61, 123001

Richards, E. A., Kellermann, K. I., Fomalont, E. B., Windhorst, R. A., & Partridge, R. B. 1997, AJ, 116, 1039.

Seljak, U., Burwell, J., & Pen, U., 2001, PRD, 63, 063001.

Springel, V., White, M., & Hernquist, L. 2001, ApJ549, 681.

Tegmark, M., Eisenstein, D.J., Hu, W., & de Oliveira-Costa, A. 2000, ApJ, 530, 133-165.

White, M., Carlstrom, J. E., Dragovan, M., & Holzapfel, W. L. 1999, ApJ, 514, 12.

White, M., Hernquist, L., & Springel, V. 2002, submitted to ApJ, astro-ph/0205437.

Zhang, P., Pen, U., & Wang, B. 2002, submitted to ApJ, astro-ph/0201375.

TABLE 1
Field Positions and Observation Times

Fields	R. A. (J2000)	Decl. (J2000)	Observation year(s)	Time (Hrs)
BDF4	00 ^h 28 ^m 04.4 ^s	+28° 23' 06"	98	77.6
HDF	12 ^h 36 ^m 49.4 ^s	+62° 12' 58"	98, 01	59.9
BDF6	18 ^h 21 ^m 00.0 ^s	+59° 15' 00"	98, 00	81.2
BDF7	06 ^h 58 ^m 45.0 ^s	+55° 17' 00"	98, 00	68.2
BDF8	00 ^h 17 ^m 30.0 ^s	+29° 00' 00"	00, 01	53.3
BDF9	12 ^h 50 ^m 15.0 ^s	+56° 52' 30"	00, 01	53.9
BDF10	18 ^h 12 ^m 37.2 ^s	+58° 32' 00"	00, 01	53.3
BDF11	06 ^h 58 ^m 00.0 ^s	+54° 24' 00"	00, 01	50.0
BDF12	06 ^h 57 ^m 38.0 ^s	+55° 32' 00"	01	54.8
BDF13	22 ^h 22 ^m 45.0 ^s	+36° 37' 00"	01	54.5

TABLE 2
Point Sources From VLA at 4.8 GHz

Field	Δ R. A. (")	Δ Decl. (")	Intrinsic Flux (μJy)
BDF4	-96.8	255.7	1230
BDF4	72.8	178.2	514
BDF4	99.9	-89.4	221
BDF4	-94.9	268.4	391
BDF4	-121.0	356.3	673
HDF	-35.0	-85.0	591
HDF	255.0	-89.8	998
HDF	178.3	-274.0	731
HDF	222.5	-86.8	345
HDF	69.1	334.1	593
HDF	-21.1	66.1	160
BDF6	-136.5	-283.5	592
BDF6	-247.2	259.9	510
BDF7	314.6	47.4	1554
BDF7	173.8	97.8	373
BDF7	253.8	-1.1	284
BDF8	-145.9	-266.1	1381
BDF8	27.6	280.9	611
BDF8	302.9	-79.5	622
BDF9	-221.9	-123.7	1500
BDF9	-192.7	215.8	1193
BDF9	245.2	-101.0	1039
BDF9	438.3	-147.3	2979
BDF10	-158.5	-165.6	1670
BDF10	-146.1	-183.9	320

TABLE 2 cont'd
Point Sources From VLA at 4.8 GHz

Field	Δ R. A. (")	Δ Decl. (")	Intrinsic Flux (μ Jy)
BDF11	474.7	471.3	24000
BDF11	87.7	77.9	246
BDF11	342.8	8.8	536
BDF11	42.5	-11.8	152
BDF12	157.4	488.5	13890
BDF12	-78.9	431.7	6244
BDF12	131.4	497.5	6230
BDF12	181.4	-49.5	477
BDF12	-154.0	299.7	1145
BDF12	225.1	-99.9	317
BDF13	-398.3	-115.1	2796
BDF13	-241.0	-256.7	1620
BDF13	260.2	300.5	1191
BDF13	-382.7	-125.9	937
BDF13	-137.4	-133.4	278
BDF13	170.9	66.7	211

TABLE 3
Image Statistics, Most Likely ΔT , and Confidence Intervals of Blank Fields in $u-v$ range $0.63 - 1.7 \text{ k}\lambda$

Field	Synthesized Beamsize (")	RMS (μ Jy beam $^{-1}$)	RMS (μ K)	ΔT (μ K)		
				Most Likely	68%	95%
BDF4	87.1×94.6	103.5	18.8	0.0	0.0 - 14.4	0.0 - 29.4
HDF	87.4×90.9	111.3	21.0	0.0	0.0 - 17.4	0.0 - 34.0
BDF6	86.6×90.9	89.9	17.3	24.0	14.2 - 34.6	2.4 - 4.46
BDF7	86.4×90.4	101.6	19.5	17.4	2.6 - 27.6	0.0 - 44.2
BDF8	84.1×87.5	108.5	22.1	0.0	0.0 - 12.6	0.0 - 24.8
BDF9	85.3×88.6	110.6	22.0	12.4	0.0 - 21.6	0.0 - 37.6
BDF10	85.8×86.8	108.6	21.9	0.0	0.0 - 15.6	0.0 - 30.0
BDF11	85.2×88.3	109.1	21.8	0.0	0.0 - 17.6	0.0 - 33.6
BDF12	87.3×88.6	112.3	21.8	35.8	23.2 - 50.2	9.8 - 67.2
BDF13	86.8×89.1	112.9	21.9	27.2	11.4 - 41.4	0.0 - 53.0
All Fields				14.2	8.2 - 19.0	0.8 - 21.8

TABLE 4
Image Statistics, Most Likely ΔT , and Confidence Intervals of Blank Fields in $u-v$ range $0.63 - 1.1 \text{ k}\lambda$

Field	Synthesized	RMS	RMS	$\Delta T_1(\mu\text{K})$		
	Beamsize('')	($\mu\text{Jy beam}^{-1}$)	(μK)	Most Likely	68%	95%
BDF4	119.7×123.3	141.7	14.4	0.0	0.0 – 13.5	0.0 – 28.2
HDF	114.2×123.8	151.8	16.1	0.0	0.0 – 21.1	0.0 – 41.1
BDF6	118.2×119.5	122.3	13.0	21.1	9.5 – 33.2	0.0 – 44.3
BDF7	117.7×121.2	138.6	14.6	23.4	5.6 – 39.1	0.0 – 57.4
BDF8	108.5×121.0	151.1	17.3	0.0	0.0 – 14.3	0.0 – 28.5
BDF9	110.6×117.7	149.7	17.2	15.2	0.0 – 24.5	0.0 – 42.9
BDF10	111.0×116.8	148.8	17.2	0.0	0.0 – 17.5	0.0 – 33.8
BDF11	110.9×117.7	149.1	17.1	0.0	0.0 – 23.6	0.0 – 44.8
BDF12	110.3×117.1	149.2	17.3	44.2	30.5 – 60.6	20.9 – 76.3
BDF13	110.8×121.0	154.2	17.3	38.8	22.9 – 56.0	7.1 – 71.8
All Fields			16.6		10.7 – 21.9	2.5 – 26.0

TABLE 5
Image Statistics, Most Likely ΔT , and Confidence Intervals of Blank Fields in $u-v$ range $1.1 - 1.7 \text{ k}\lambda$

Field	Synthesized	RMS	RMS	$\Delta T_2(\mu\text{K})$		
	Beamsize('')	($\mu\text{Jy beam}^{-1}$)	(μK)	Most Likely	68%	95%
BDF4	69.5×77.4	153.2	42.7	33.2	5.3 – 49.6	0.0 – 69.0
HDF	69.3×75.7	164.5	47.0	26.5	0.0 – 43.2	0.0 – 68.4
BDF6	69.5×74.4	132.7	38.5	10.7	0.0 – 32.9	0.0 – 57.5
BDF7	69.6×73.7	149.2	43.6	2.2	0.0 – 38.4	0.0 – 65.3
BDF8	67.6×74.6	155.8	46.3	0.0	0.0 – 29.6	0.0 – 55.8
BDF9	69.8×72.0	164.1	49.0	0.0	0.0 – 34.7	0.0 – 61.8
BDF10	70.6×71.1	159.0	47.5	0.0	0.0 – 30.7	0.0 – 58.3
BDF11	68.8×73.7	159.9	47.3	0.0	0.0 – 29.6	0.0 – 56.9
BDF12	70.3×72.2	170.7	50.4	0.0	0.0 – 36.3	0.0 – 64.2
BDF13	69.6×75.0	165.7	47.6	0.0	0.0 – 29.8	0.0 – 57.4
All Fields			0.0		0.0 – 14.6	0.0 – 26.5

TABLE 6
The Effect of point source model on ΔT_1

VLA Flux Limit	Most likely	$\Delta T_1(\mu\text{K})$			Confidence
		68%	95%	$\Delta T_1 > 0$	
none	17.7	12.1 – 22.9	4.7 – 27.6	98.8%	
$> 12\sigma$	16.7	10.9 – 21.7	2.8 – 26.0	98.1%	
$> 8\sigma$	17.1	11.2 – 22.3	3.7 – 26.7	98.3%	
$> 6\sigma$	16.4	10.5 – 21.7	3.1 – 25.7	97.9%	

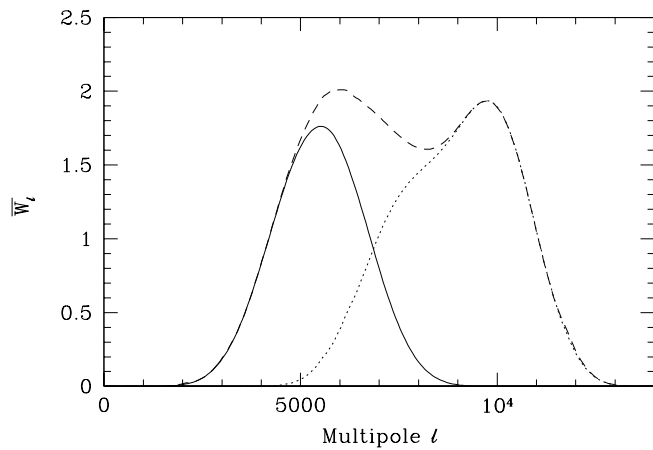


Fig. 1.— The “data weighted” window functions \overline{W}_ℓ . The solid line corresponds to data in the $u-v$ range $0.63 - 1.1 \text{ k}\lambda$, the dotted line corresponds to data in the $u-v$ range $1.1 - 1.7 \text{ k}\lambda$ and the dashed line corresponds to data in the $u-v$ range $0.63 - 1.7 \text{ k}\lambda$. The dual peaks are due to the bimodal distribution of baselines in the compact BIMA configuration.

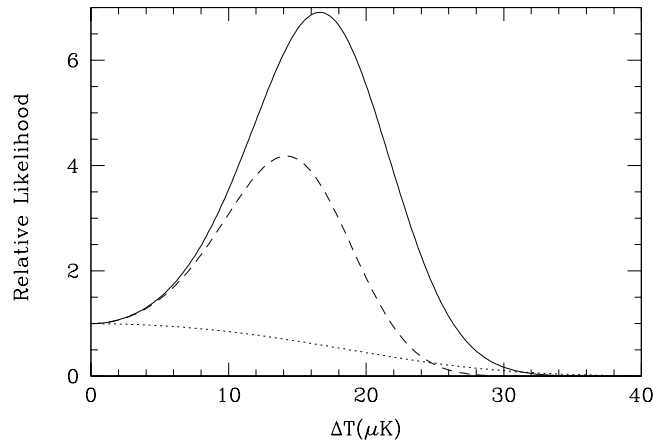


Fig. 2.— The relative likelihood that the observed signal in the ten combined fields is described by flat band power with amplitude ΔT . The solid line corresponds to an analysis of ΔT_1 , with data in the $u-v$ range $0.63 - 1.1 \text{ k}\lambda$, the dotted line corresponds to an analysis of ΔT_2 , with data in the $u-v$ range $1.1 - 1.7 \text{ k}\lambda$ and the dashed line corresponds to an analysis of ΔT , with data in the $u-v$ range $0.63 - 1.7 \text{ k}\lambda$.

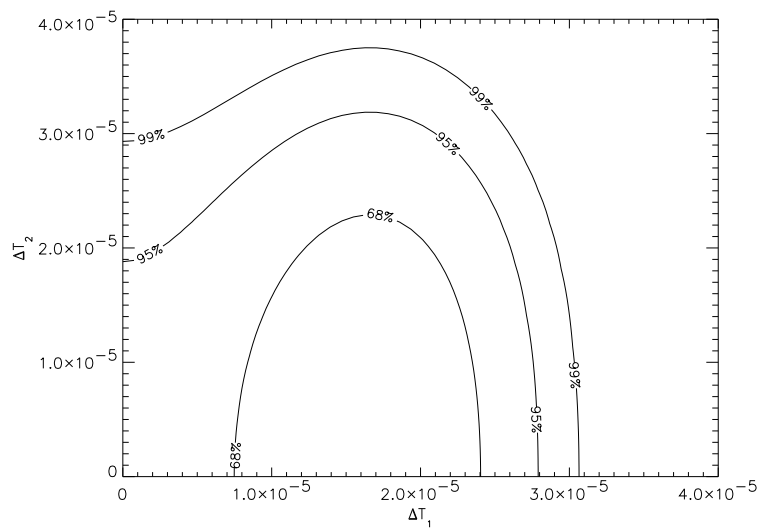


Fig. 3.— The likelihood that the observed signal in the ten combined fields is described by flat band power with amplitude ΔT_1 , ΔT_2 . Contours represent confidence intervals.

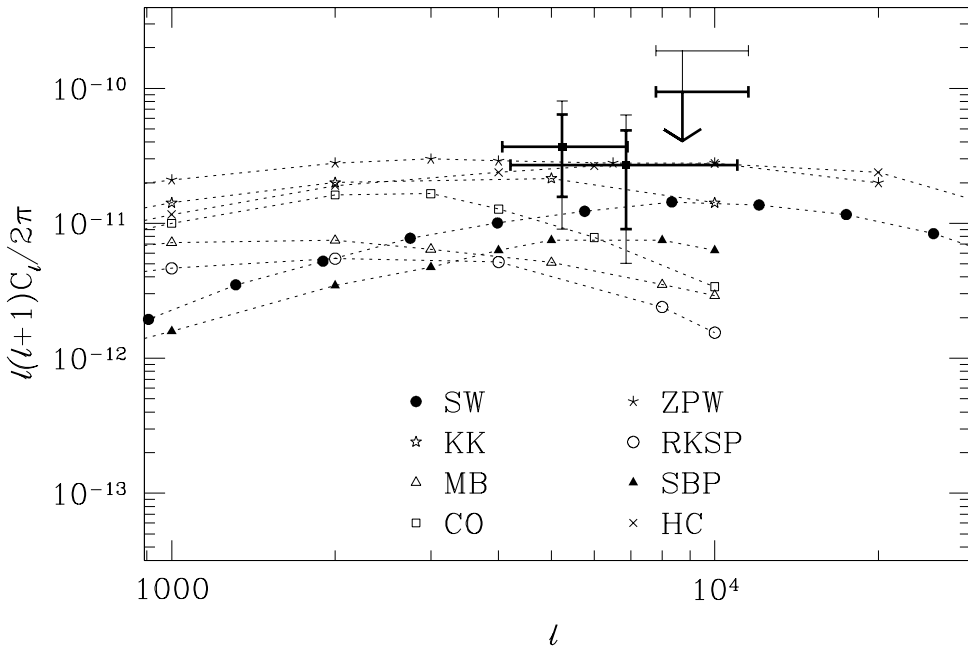


Fig. 4.— Published estimates of the thermal SZ power spectrum compared to the result of this work. The results of the BIMA experiment are expressed with 68% confidence intervals for $\ell_{eff} = 5237$ and for $\ell_{eff} = 6864$ and a 95% upper limit for $\ell_{eff} = 8748$. Extended error bars represent the estimated effect of non-Gaussian sample variance. Other symbols give computations by the following authors: SW (Springel, White, & Hernquist 2000), KK (Komatsu & Kitayama 1999), MB (Molnar & Birkinshaw 2000), CO (Cooray 2000), ZPW (Zhang et al. 2002), RKSP (Refregier et al. 2000), SBP (Seljak et al. 2000), and HC (Holder & Carlstrom 1999).